Draft version May 20, 2019
Typeset using LaTeX default style in AASTeX62

The Empirical Delay Time Distributions of Type Ia Supernovae From Galaxy and Cosmic Star Formation Histories

L.-G. Strolger, Steven Rodney, Camila Pacifici, and et al.

ABSTRACT

blah, blah, blah ...

1. INTRODUCTION

The understanding of cosmic type Ia supernova (SN Ia) rates has critical importance to understanding galaxy evolutionary feedback mechanisms, cosmic iron enrichment and α-process element enrichment histories (see Maoz & Graur 2017), and perhaps most importantly, constraining the physical mechanisms of SN Ia progenitors, and therefore providing some constraint on the systematic uncertainties of dark energy. However, determining precise SN Ia rates and rate histories, and establishing the connections of those rates to host (and cosmic) properties has been a slog.

In tracing the cosmic (or volumetric) rate history, the first precise measures of the local ($z \approx 0.0$) rate came in the early 1990s (cf. Cappellaro et al. 1993; Cappellaro et al. 1999), and the first measures beyond the local Hubble flow came in the early 2000s, many as collateral results of the dark energy experiments (Riess et al. 1998; Perlmutter et al. 1999). Since then, there have been several measures of the volumetric SN Ia rate at various redshifts by various groups, a collection of which is shown in Table 1 and Figure 1. Not all rate measures have been in total agreement with one another (see the large scatter just below $z \sim 0.5$), with the reasons as to why ranging from statistical variation, to differences on the treatment of declining SNe, to ultimately differences in the assessment of effective survey duration, through modeling and through simulation. It is left to a future study to attempt a reanalysis of some (or all) of the reported rate measures in at least a self-consistent assessment to reduce some of the unreported systematic uncertainties. However for the time being, it is probably best to consider each published rate as a valid measure that may (or may not) have misestimated uncertainties.

Table 1. Volumetric SN Ia Rates Used in this Work

Redshift	$R_{\rm Ia}$[a]	Stat. Uncertainty	Sys. Uncertainty	Source
0.01	0.28	$^{+0.09}_{-0.09}$	$^{+0.0}_{-0.0}$	Cappellaro et al. (1999)
0.03	0.28	$^{+0.11}_{-0.11}$	$^{+0.0}_{-0.0}$	Mannucci et al. (2005)
0.0375	0.278	$^{+0.112}_{-0.083}$	$^{+0.015}_{-0.00}$	Dilday et al. (2010)
0.1	0.259	$^{+0.052}_{-0.044}$	$^{+0.028}_{-0.001}$	Dilday et al. (2010)
0.10	0.32	$^{+0.15}_{-0.15}$	$^{+0.0}_{-0.0}$	Madgwick et al. (2003)
0.10	0.55	$^{+0.50}_{-0.29}$	$^{+0.20}_{-0.20}$	Cappellaro et al. (2015)
0.11	0.37	$^{+0.10}_{-0.10}$	$^{+0.0}_{-0.0}$	Strolger (2003)
0.13	0.20	$^{+0.07}_{-0.07}$	$^{+0.05}_{-0.05}$	Blanc et al. (2004)
0.15	0.307	$^{+0.038}_{-0.034}$	$^{+0.035}_{-0.005}$	Dilday et al. (2010)
0.15	0.32	$^{+0.23}_{-0.23}$	$^{+0.23}_{-0.06}$	Rodney & Tonry (2010)
0.16	0.14	$^{+0.09}_{-0.09}$	$^{+0.06}_{-0.12}$	Perrett et al. (2012)
0.2	0.348	$^{+0.032}_{-0.030}$	$^{+0.082}_{-0.007}$	Dilday et al. (2010)
0.20	0.20	$^{+0.08}_{-0.08}$	$^{+0.0}_{-0.0}$	Horesh et al. (2008)
0.25	0.36	$^{+0.60}_{-0.26}$	$^{+0.12}_{-0.35}$	Rodney et al. (2014)
0.25	0.365	$^{+0.031}_{-0.028}$	$^{+0.182}_{-0.012}$	Dilday et al. (2010)
0.25	0.39	$^{+0.13}_{-0.12}$	$^{+0.10}_{-0.10}$	Cappellaro et al. (2015)

Table 1 continued on next page

Table 1 *(continued)*

Redshift	$R_{\rm Ia}$[a]	Stat. Uncertainty	Sys. Uncertainty	Source
0.26	0.28	$^{+0.07}_{-0.07}$	$^{+0.06}_{-0.07}$	Perrett et al. (2012)
0.30	0.34	$^{+0.16}_{-0.15}$	$^{+0.0}_{-0.0}$	Botticella et al. (2008)
0.30	0.434	$^{+0.037}_{-0.034}$	$^{+0.396}_{-0.016}$	Dilday et al. (2010)
0.35	0.34	$^{+0.19}_{-0.19}$	$^{+0.19}_{-0.03}$	Rodney & Tonry (2010)
0.35	0.36	$^{+0.06}_{-0.06}$	$^{+0.05}_{-0.06}$	Perrett et al. (2012)
0.42	0.46	$^{+0.42}_{-0.32}$	$^{+0.10}_{-0.13}$	Graur et al. (2014)
0.44	0.262	$^{+0.229}_{-0.133}$	$^{+0.059}_{-0.120}$	Okumura et al. (2014)
0.45	0.31	$^{+0.15}_{-0.15}$	$^{+0.15}_{-0.04}$	Rodney & Tonry (2010)
0.45	0.36	$^{+0.06}_{-0.06}$	$^{+0.04}_{-0.05}$	Perrett et al. (2012)
0.45	0.52	$^{+0.11}_{-0.13}$	$^{+0.16}_{-0.16}$	Cappellaro et al. (2015)
0.46	0.48	$^{+0.17}_{-0.17}$	$^{+0.0}_{-0.0}$	Tonry et al. (2003)
0.47	0.42	$^{+0.06}_{-0.06}$	$^{+0.13}_{-0.09}$	Neill et al. (2006)
0.47	0.80	$^{+0.37}_{-0.27}$	$^{+1.66}_{-0.26}$	Dahlen et al. (2008)
0.55	0.32	$^{+0.14}_{-0.14}$	$^{+0.14}_{-0.07}$	Rodney & Tonry (2010)
0.55	0.48	$^{+0.06}_{-0.06}$	$^{+0.04}_{-0.05}$	Perrett et al. (2012)
0.55	0.52	$^{+0.10}_{-0.09}$	$^{+0.0}_{-0.0}$	Pain et al. (2002)
0.65	0.48	$^{+0.05}_{-0.05}$	$^{+0.04}_{-0.06}$	Perrett et al. (2012)
0.65	0.49	$^{+0.17}_{-0.17}$	$^{+0.17}_{-0.08}$	Rodney & Tonry (2010)
0.65	0.69	$^{+0.19}_{-0.18}$	$^{+0.27}_{-0.27}$	Cappellaro et al. (2015)
0.74	0.79	$^{+0.33}_{-0.41}$	$^{+0.0}_{-0.0}$	Graur et al. (2011)
0.75	0.51	$^{+0.27}_{-0.19}$	$^{+0.23}_{-0.19}$	Rodney et al. (2014)
0.75	0.58	$^{+0.06}_{-0.06}$	$^{+0.05}_{-0.07}$	Perrett et al. (2012)
0.75	0.68	$^{+0.21}_{-0.21}$	$^{+0.21}_{-0.14}$	Rodney & Tonry (2010)
0.80	0.839	$^{+0.230}_{-0.185}$	$^{+0.060}_{-0.120}$	Okumura et al. (2014)
0.83	1.30	$^{+0.33}_{-0.27}$	$^{+0.73}_{-0.51}$	Dahlen et al. (2008)
0.85	0.57	$^{+0.05}_{-0.05}$	$^{+0.06}_{-0.07}$	Perrett et al. (2012)
0.85	0.78	$^{+0.22}_{-0.22}$	$^{+0.22}_{-0.16}$	Rodney & Tonry (2010)
0.94	0.45	$^{+0.22}_{-0.19}$	$^{+0.13}_{-0.06}$	Graur et al. (2014)
0.95	0.76	$^{+0.25}_{-0.25}$	$^{+0.25}_{-0.26}$	Rodney & Tonry (2010)
0.95	0.77	$^{+0.08}_{-0.08}$	$^{+0.10}_{-0.12}$	Perrett et al. (2012)
1.05	0.79	$^{+0.28}_{-0.28}$	$^{+0.28}_{-0.41}$	Rodney & Tonry (2010)
1.1	0.74	$^{+0.12}_{-0.12}$	$^{+0.10}_{-0.13}$	Perrett et al. (2012)
1.14	0.705	$^{+0.239}_{-0.183}$	$^{+0.102}_{-0.103}$	Okumura et al. (2014)
1.21	1.32	$^{+0.36}_{-0.29}$	$^{+0.38}_{-0.32}$	Dahlen et al. (2008)
1.23	0.84	$^{+0.25}_{-0.28}$	$^{+0.0}_{-0.0}$	Graur et al. (2011)
1.25	0.64	$^{+0.31}_{-0.22}$	$^{+0.34}_{-0.23}$	Rodney et al. (2014)
1.59	0.45	$^{+0.34}_{-0.22}$	$^{+0.05}_{-0.09}$	Graur et al. (2014)
1.61	0.42	$^{+0.39}_{-0.23}$	$^{+0.19}_{-0.14}$	Dahlen et al. (2008)
1.69	1.02	$^{+0.54}_{-0.37}$	$^{+0.0}_{-0.0}$	Graur et al. (2011)
1.75	0.72	$^{+0.45}_{-0.30}$	$^{+0.50}_{-0.28}$	Rodney et al. (2014)
2.25	0.49	$^{+0.95}_{-0.38}$	$^{+0.45}_{-0.24}$	Rodney et al. (2014)

[a] In units 10^{-4} yr^{-1} Mpc^{-3} h_{70}^{3}

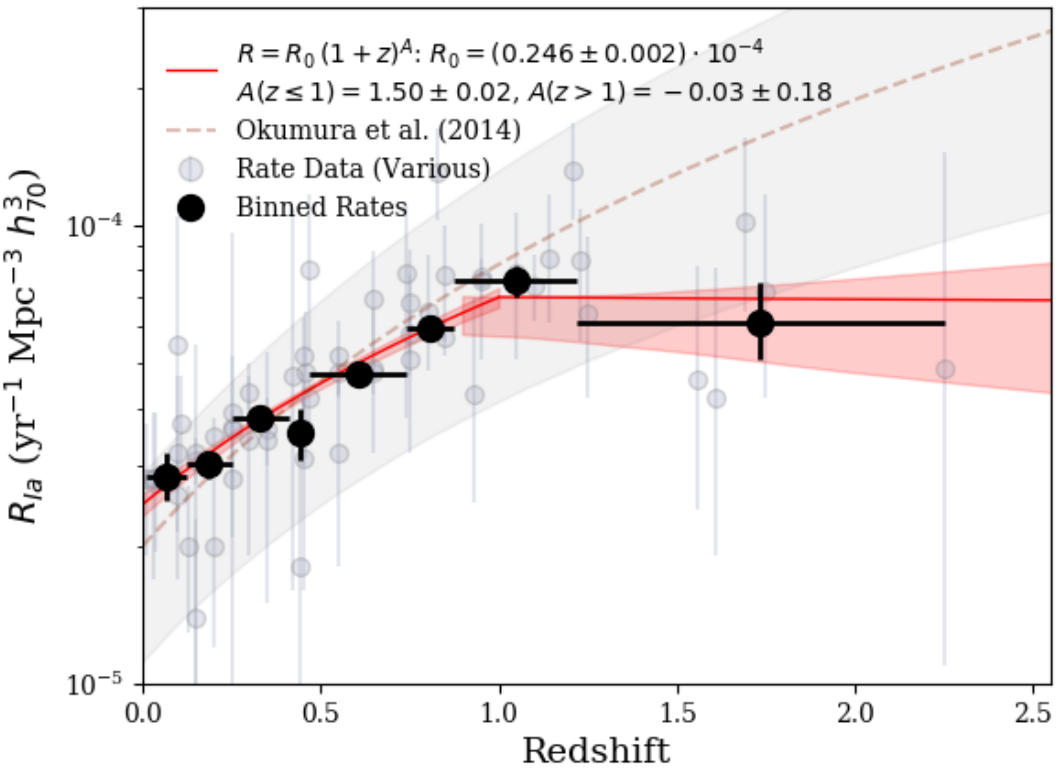

Figure 1. Type Ia supernova volumetric rate measures from various sources in the literature (gray points, see Table 1 for their sources), and binned (black points, see Table 2), largely for illustration. The solid red lines show a broken power-law fit to the data in redshift space. The dashed red line (and associated uncertainty region, in gray) is from Okumura et al. (2014).

From this rate history and a comparison to the cosmic star formation history, one can reconstruct (or infer) the distribution of times from SN progenitor formation to explosion, assuming the mechanism is ubiquitous enough that it can be characterized by a singular distribution of delay times. It has been long expected that this 'delay time distribution' will distinguish between single-degenerate (Whelan & Iben 1973; Nomoto 1982) and double-degenerate (Iben & Tutukov 1984; Webbink 1984) models, depending on what the models for each of these scenarios would expect (see Section 2.3 for more details).

Another method in reconstructing delay times results from an analysis of the star-formation histories in individual host galaxies (Brandt et al. 2010; Maoz et al. 2011, 2012), under the same assumptions as above. Rather than using bulk star formation properties, averaged in large temporal bins (by redshift), the method uses spectral analysis tools to reconstruct star formation histories, then determine the contributions (in broad times bins) from a delay time distribution that maximize the likelihood that the hosts would produce SNe Ia in the duration of a survey. However, to date, this method has not been done to redshifts $z \sim 1$, the results in clustered and field environments are different, and the results are dependent on the assumed model.

In this paper, we present a analysis of delay time distributions using these two separate methods, from a comparison of volumetric SN Ia rates to cosmic star formation rates (Section 2), and a maximized likelihood method from SN Ia host star formation histories (Section 3). In Section 4 we discuss the results from each of these methods and put them into context with results from other work, and into context with binary synthesis models.

2. DELAY TIME DISTRIBUTIONS FROM VOLUMETRIC SN IA RATES AND THE COSMIC STAR FORMATION HISTORY

The various SN Ia volumetric rate measurements are shown in Table 1 and Figure 1. For illustration purposes only, here and through out this manuscript, we bin the rate data into 8 quantiles of nearly equal number of measures and

present those binned measures, weighted by reported statistical uncertainties only, in Figure 1 and in Table 2. None of the analysis presented herein was performed on the binned measures, rather directly on the rate values themselves.

Table 2. Binned volumetric SN Ia rates, with statistical uncertainties.

Redshift	$R_{\rm Ia}$ [a]	$N_{\rm measures}$
0.07 ± 0.06	$0.28^{+0.04}_{-0.03}$	7
0.19 ± 0.06	$0.30^{+0.02}_{-0.02}$	6
0.33 ± 0.08	$0.38^{+0.02}_{-0.02}$	8
0.44 ± 0.03	$0.35^{+0.05}_{-0.04}$	6
0.61 ± 0.14	$0.47^{+0.03}_{-0.03}$	9
0.81 ± 0.07	$0.60^{+0.04}_{-0.04}$	7
1.05 ± 0.17	$0.76^{+0.06}_{-0.06}$	7
1.73 ± 0.52	$0.61^{+0.14}_{-0.10}$	7

[a] In units 10^{-4} yr^{-1} Mpc^{-3} h^3_{70}

It would be reasonable to assume the volumetric rates follow a broken power law evolution with redshift, $R_{\rm Ia} = R_0\,(1+z)^A$, where the power-law slope at $z < 1$ is $A = 1.50 \pm 0.02$ (with $R_0 = 2.47 \pm 0.02 \times 10^{-5}$ yr^{-1} Mpc^{-3} h^3_{70}), which flattens substantially to $A = 0.0 \pm 0.2$ at redshifts greater than 1, as is shown in Figure 1. This is broadly consistent with the power-law fit from Okumura et al. (2014), especially to $z \lesssim 1$. The locus is also consistent with the volumetric SN Ia rate at $z \approx 0$ converted by Li et al. (2011) to $2.7 \pm 0.3 \times 10^{-5}$ yr^{-1}. While the broken power-law model is useful for predicting yields from volumetric surveys, e.g., for the Wide Field InfraRed Survey Telescope (*WFIRST,* Hounsell et al. 2018) and the Large Synoptics Survey Telescope (LSST), it does not inherently reveal much on the nature of SN Ia progenitor mechanisms. This is better done through an assessment of delay-time distributions.

For these types of analyses, the standard assumption is that the stellar death rate (or supernova rate) is related to the stellar birth rate, convolved with some delay-time distribution that contains all the temporal factors of stellar evolution (e.g., main sequence lifetime, etc.) and binary star evolution (e.g., accretion rates or merger times). Two additional terms include the fraction of the initial mass function (or IMF) that the progenitors of SNe Ia arise from, presumably $3-8\,{\rm M}_\odot$ zero-age main sequence stars, as discussed in Section 2.1, and the fraction of that population that are actually capable of producing events, as not all progenitor stars are necessarily in binary systems, or presumably the right type of binary systems to successfully result in SNe Ia.

We can relate volumetric SN Ia rate history to the cosmic star formation history($\dot\rho_\star$) in a similar way, expressed mathematically by,

$$R_{\rm Ia}(t) = h^2\,k\,\varepsilon\left[\dot\rho_\star(t) * \Phi(t)\right], \tag{1}$$

where $\Phi(t)$ is the delay-time distribution of SNe Ia, k is the fraction of the IMF (by mass) responsible for SN Ia progenitors, ε is the fraction of that population that are ultimately successful in producing SNe Ia, and t is the forward-moving clock of the universe. The two factors of the dimensionless Hubble constant arise from the determination of stellar mass formation from luminosity in $\dot\rho_\star(t)$ (Croton 2013).

2.1. *The Fraction of Stars Responsible for SNe Ia*

Dissecting each of these terms, k is perhaps the easiest to approximate. The progenitors of SNe Ia have traditionally been CO WD which acquire sufficient mass to approach or exceed the Chandrasekhar mass limit, $M_{ch} = 1.44\,M_\odot$. To only marginally achieve this, they can either start at sufficiently high mass to require only a small amount of accretion from a nearby companion (typically single-degenerate, or SD, scenarios), or as a pair of WD that have combined in mass to meet this criterion (the double-degenerate, or DD, scenario) setting an even lower constraint (see Maoz et al. 2013, for a review). In the case of DD mergers, WD mass distributions are strongly peaked around $M_{\rm WD} \approx 0.6 \pm 0.1\,M_\odot$ (Catalán et al. 2008), in which a pair drawn from such distribution may be satisfactorily close to the ignition threshold of a carbon core for a non-rotating CO WD, approximately $1.38\,M_\odot$ (Arnett 1969; Nomoto 1982). Initial-Final Mass relations (e.g., Catalán et al. 2008; Cummings et al. 2018) would correspond these to zero-age main-sequence (ZAMS) masses of approximately $3\,M_\odot$, but no less than approximately $2.5\,M_\odot$. The same Initial-Final Mass relations would

Table 3. Cosmic Star Formation History Parameter Fits

	A	B	C	D
Madau & Dickinson (2014) only	0.013 ± 0.001	2.6 ± 0.1	3.2 ± 0.2	6.1 ± 0.2
Driver et al. (2018)[a] only	0.014 ± 0.001	2.5 ± 0.2	3.3 ± 0.3	6.2 ± 0.3
All Combined Data	0.0134 ± 0.0009	2.55 ± 0.09	3.3 ± 0.2	6.1 ± 0.2

[a]Corrected for dust attenuation.

suggest that a WD essentially at M_{ch} would fall just below $8\,M_\odot$ ZAMS. Similarly, simulations show that the lowest mass in which C ignition is still possible is around $6-8\,M_\odot$ Chen et al. (2014); Denissenkov et al. (2015), but likely no more than $\sim 11\,M_\odot$ (Takahashi et al. 2013), above which an electron-capture-induced collapse mechanism begins, marking the onset of core-collapse supernovae.

It is reasonable, therefore, to assume a progenitor mass range of about $3-8\,M_\odot$ ZAMS. From a numerical assessment of these stars, assuming they fall within an IMF that is a power-law distribution by mass (in this initial mass range) with $\alpha \approx -2.3$ (Salpeter 1955; Kroupa 2001), one would expect

$$k = \frac{\int_{3M_\odot}^{8M_\odot} \xi(M)\,dM}{\int_{0.1M_\odot}^{125M_\odot} M\,\xi(M)\,dM} = 0.021^{+33\%}_{-24\%}\,M_\odot^{-1}, \tag{2}$$

where error in k is driven more by choices in the upper and lower value in the selected mass range of SN Ia progenitors than by the choice in IMF model, as detailed above.

The fraction of CO WDs that are ultimately successful in making SNe Ia is hard to determine, as we do not quite yet know the details of the progenitor mechanism or mechanisms. Estimates swing rather wildly from (perhaps) as low as 1 in 200 (Breedt et al. 2017) to as optimistic as 1 in 40 (Maoz & Mannucci 2012). There is at least strong consensus that accretion on to a CO WD is essential, but very different plausible WD close binary scenarios from at least a theoretical standpoint (Nelemans et al. 2001a,b). The binary fractions of WDs has been recently estimated from the the ESO-VLT Supernova-Ia Progenitor Survey (Napiwotzki et al. 2007, SPY) show close double WD systems may have $\varepsilon_{\rm bin} \simeq 0.1 \pm 0.02$ (Maoz & Hallakoun 2017). It is not likely all of these successfully yield SNe Ia as their merger rates in the MW are at least a magnitude higher than best estimates of the SN Ia rate in our galaxy, and presumably some of these will form AM CVn and R Corona Borealis stars, but at least it could be treated as an upper limit on ε.

2.2. *The Star Formation Density History*

The cosmic star formation history (CSFH), at least to $z < 5$ or over 90% of the history of the universe, is fairly well understood, with Madau & Dickinson (2014; MD14 hereafter) providing one of the most complete compilations. More recently, the CSFH derived from the combined GAMA, G10-COSMOS, and 3D-HST datasets by Driver et al. (2018), in a quasi-homogeneous analysis over a larger area, provides a dataset with greatly reduced uncertainties per datum, but fewer data than presented in the MD14 compendium (see Figure 2). We combine the MD14 and Driver et al. (2018) data, with additional star-formation rate densities from Bouwens et al. (2015) and Khusanova et al. (2019), to arrive at today's compendium CSFH using the parameterization,

$$\dot\rho_\star(z) = \frac{A\,(1+z)^C}{((1+z)/B)^D + 1}. \tag{3}$$

However, to do so we correct the Driver et al. (2018) data for dust attenuation following the prescription in MD14, by applying

$$\dot\rho_\star(z) = h^3 \left[1 + 10^{0.4\cdot A_{\rm FUV}(z)}\right] \dot\rho_{\star,\rm uncorrected}(z), \tag{4}$$

where it is assumed $A_{\rm FUV}(z)$ has the same functional form of Equation 3, with $A = 1.4\pm0.1$, $B = 3.5\pm0.4$, $C = 0.7\pm0.2$, and $D = 4.3 \pm 0.7$ as determined from the $A_{\rm FUV}(z)$ data from MD14. We then fit Equation 3 to the combined CSFH datasets, resulting in Levenberg-Marquardt least-squares solution parameters which are extraordinarily constrained, as shown in Table 3 and Figure 2.

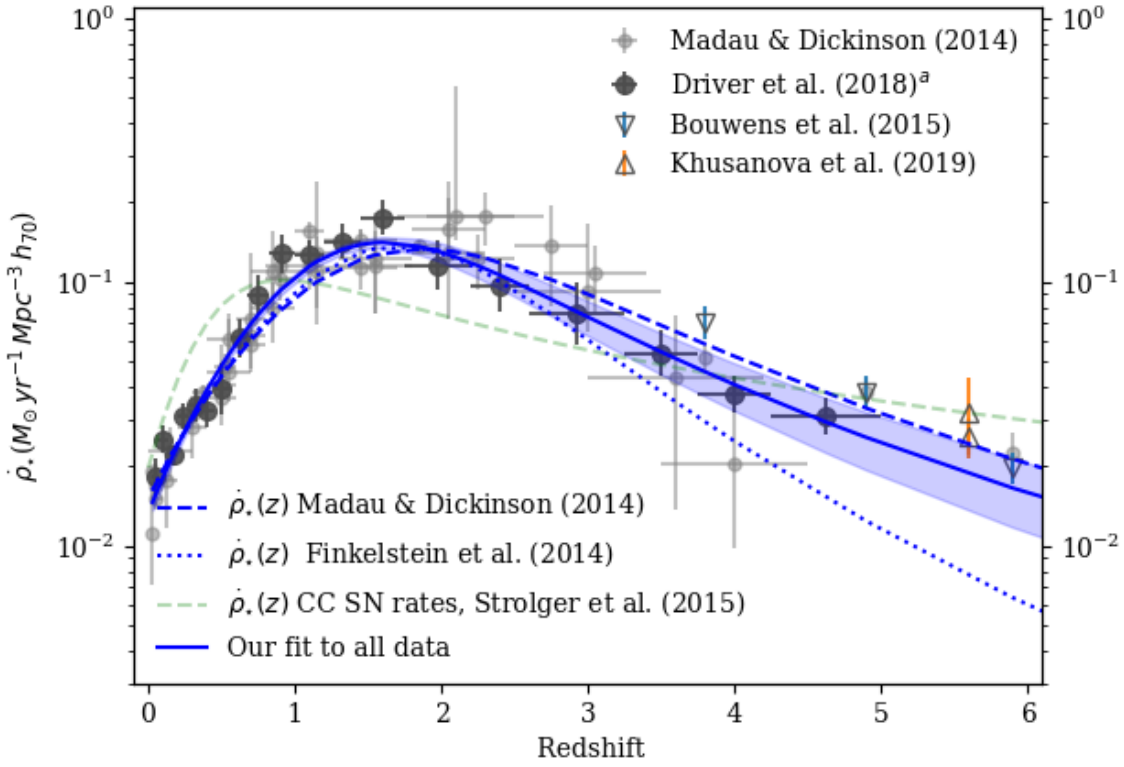

Figure 2. Shown are a compendium of cosmic star formation histories, from Madau & Dickinson (2014), Driver et al. (2018; [a]-dust corrected), Bouwens et al. (2015), and Khusanova et al. (2019). Dashed and dotted lines are previous models from Madau & Dickinson (2014), Finkelstein et al. (2014), Strolger et al. (2015), as indicated. Solid blue line (and blue shaded region) represent our best-fit model to the compendium of data.

2.3. *SN Ia Progenitor Delay-Time Distribution Models*

Theoretical delay time distributions result from analyses of binary population synthesis, and from physical bases (see Wang & Han 2012, for a review). In the SD scenario, details ranging from composition of the companion donor star (H or He) to the mass-accretion efficiency lead to rather large variations in the expected delay time distributions Nelemans et al. (2013). However DD models are in reasonable agreement with one another, largely because the scenario is governed by the loss of angular momentum due in the radiation of gravitational waves. The timescales involved depend on the initial separations of the WDs. If it is assumed WD binaries follow a power-law of radial distributions, $\Phi(r) = r^{\beta}$, with power $\beta \approx -1$ (Öpik 1924), as is supported by SPY close WD systems with separations distributed following $\beta = -1.3 \pm 0.2$ (Maoz & Hallakoun 2017), the resultant delay time distribution will also follow a power-law distribution, $\Phi(t) = t^{\beta}$, with a power close to $\beta \approx -1$.

Delay-time distribution recovery methods based on matching theoretical $\Phi(t)$ to CSFHs and SN Ia volumetric rates has been hampered largely by the uncertainty in the latter two (Dahlen et al. 2008; Strolger et al. 2010; Graur et al. 2014; Rodney et al. 2014), specifically in the uncertainty in the SN Ia rate above 'SN high noon' (around $z \sim 1$), and the uncertainty in CSFH above 'cosmic high noon' (around $z \sim 2$). It seems now, however, that those uncertainties have reduced to the point of making a $\Phi(t)$ reconstruction viable.

Following the methodology in Strolger et al. (2010), we can test the intrinsic shape of the delay time distribution using a robustly tunable unimodal model, then compare the results to the shapes of the theoretical distributions for SD and DD models. We use the skew-normal $\Phi(t)$ function, defined as:

$$\Phi(t) = \frac{1}{\omega\pi}\,\exp\left(\frac{-(t-\xi)^2}{2\omega^2}\right)\int_{-\infty}^{\alpha\left(\frac{t-\xi}{\omega}\right)}\exp\left(\frac{-t'^2}{2}\right)dt', \tag{5}$$

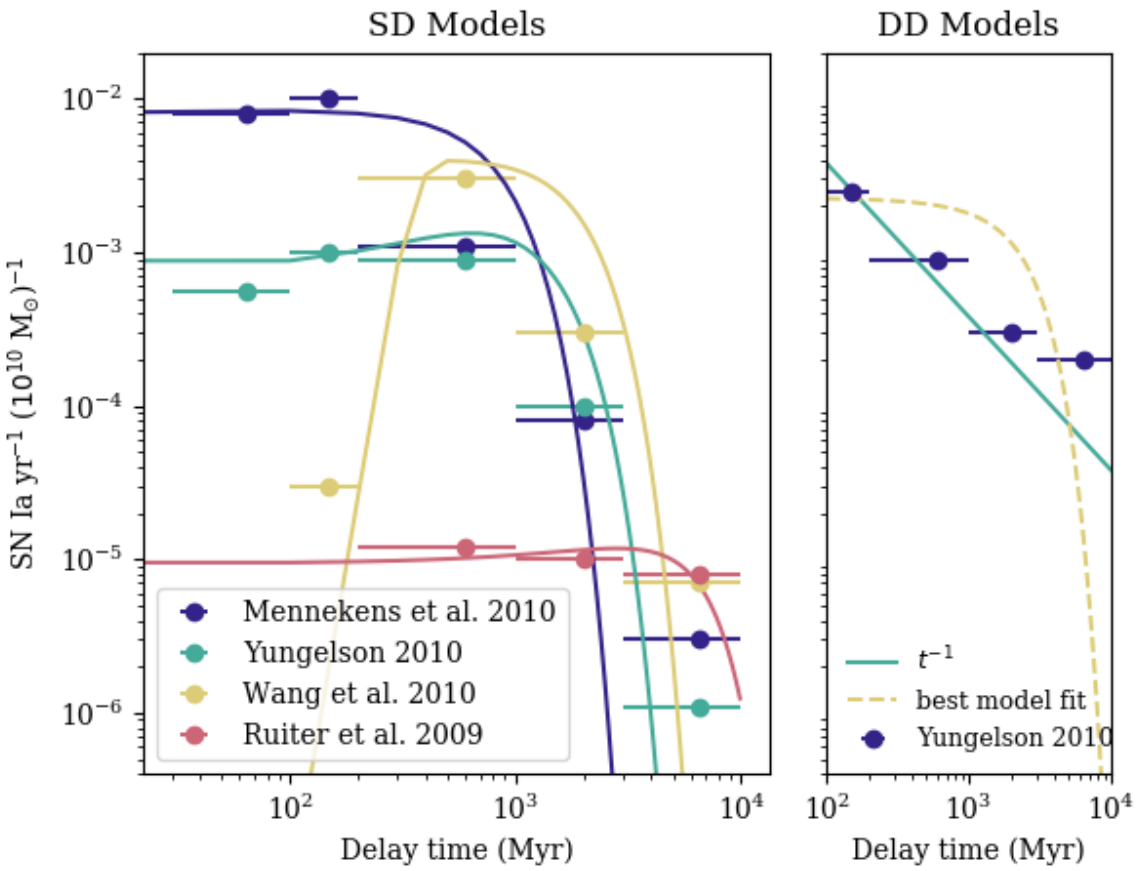

Figure 3. Examples of delay-time distributions from binary population synthesis analyses for SD (left) and DD (right) scenarios, from Nelemans et al. (2013). Shown also are fits to these models using the function described in Equation 5, tuning dependent variables ξ, ω, and α.

where location (ξ),[1] width (ω^2), and shape (α)[2] are the dependent variables. Figure 3 demonstrates the flexibility of the function in reproducing various model SD and DD from Nelemans et al. (2013). As can be seen, the defined function is very good at reproducing the shapes of various binary population synthesis models, particularly SD distributions, and fairly reasonable in fitting DD distributions, although it should be emphasized that due to the exponential nature of the function, has trouble *exactly* reproducing the shape of a distribution that is intrinsically a power-law, a point that will be revisited in Section 4.

Either through an optimized fit of the fuctional parameters (ξ, ω, and α), or through a Markov-chain monte carlo (MCMC), we can test model $\Phi(t)$ through Equation 1 in comparison to the volumetric rate measurements.

2.4. *The Optimized Solution*

We apply a maximum likelihood estimation method to determine the best-fit skew normal delay time model to Equation 1 using an optimized method described in Hogg et al. (2010). For simplicity, we assume that the errors of all survey data are gaussian in nature, but may be underestimated by some factor (f), which is justified even if only by the fact that we are using just the statistical error reported for each rate value. As follows, we adopt the likelihood function to be:

$$\ln p(y|x,\sigma,\varepsilon,\xi,\omega,\alpha,f) = -\frac{1}{2}\sum_i \left\{ \frac{[R_{\mathrm{Ia},i} - R_{\mathrm{Ia}}(t_i;\varepsilon,\xi,\omega,\alpha)]^2}{s_i^2} + \ln(2\pi s_i^2) \right\}, \quad (6)$$

[1] Different from the initial mass function, $\xi(M)$.
[2] Different from the initial mass function power-law slope at the low-mass end.

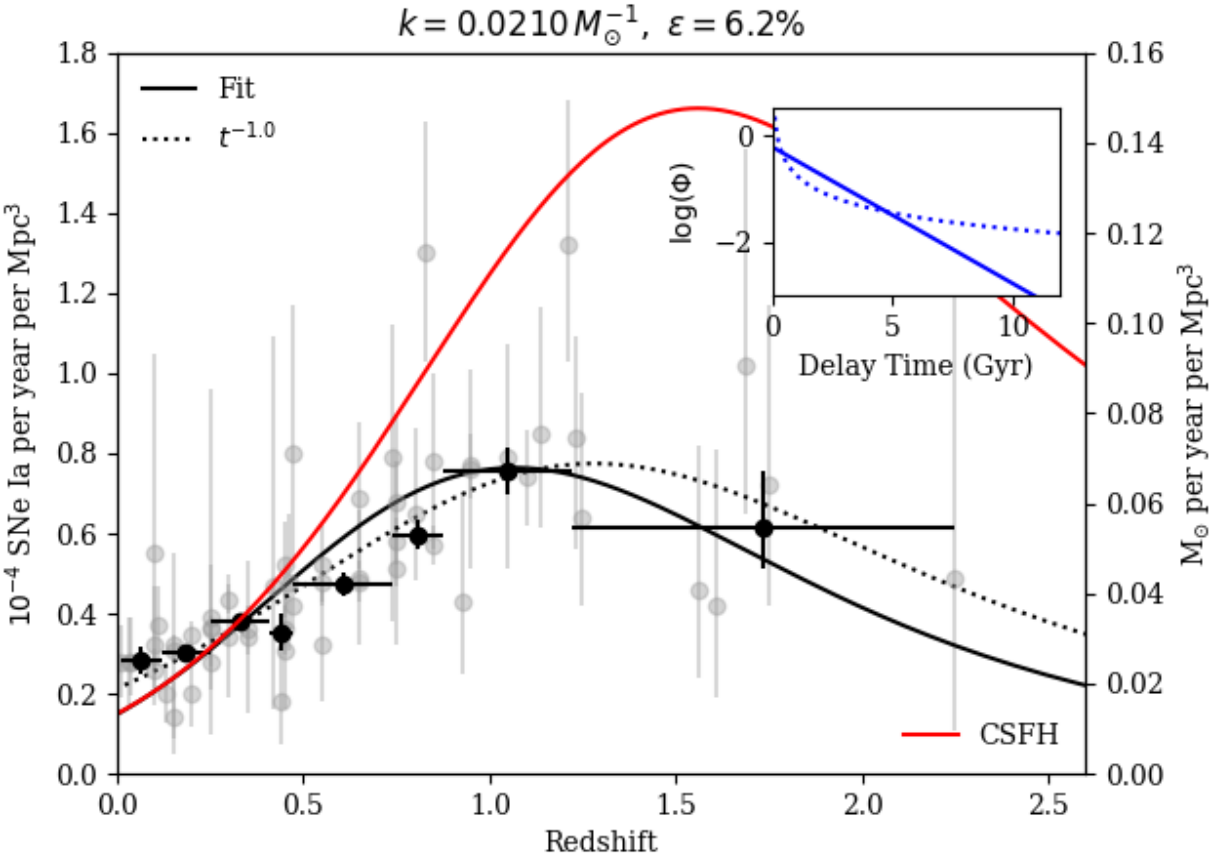

Figure 4. In addition to rate values shown in previous figures, the $R_{\rm Ia}(z)$ model results of from optimal parameter fitting of the unimodal $\Phi(\tau)$ model is shown (solid black line) in comparison to a $\beta = -1$ power-law $\Phi(\tau)$ (dashed black line). The inset shows the comparison of the two $\Phi(\tau)$ models. The CSFH is shown on in red, and along the secondary ordinate.

where,

$$s_i^2 = \sigma_i^2 + f^2\, R_{\rm Ia}(t_i; \varepsilon, \xi, \omega, \alpha)^2, \tag{7}$$

$R_{{\rm Ia},i}$ is the various independent rate measures, and $R_{\rm Ia}(t_i)$ is the parameter-dependent model predictions at the cosmic time of the various rate measures. We then find the optimal parameters which maximize this likelihood. As for priors, we require the successful fraction of progenitors to be between zero and unity ($0 < \varepsilon < 1$), that the width parameter can only be positive ($\omega > 0$), and the that underestimation fraction can only be between approximately zero and unity ($-4 < \ln f < 0$). Otherwise, we apply rather loose and arbitrary bounds of $-2000 < \xi < 2000$ and $-500 < \alpha < 500$.

The results of this optimized fit are shown in Figure 4 and tabulated in Table 4. While the optimization results a model that isconsistent with the t^{-1} model, it is not directly possible to estimate errors on the best-fit parameters, or the range of validity via this maximum likelihood optimization method.

Table 4. Results for Skew-normal Model fits

Model test	$\ln \varepsilon$	ξ	ω	α	$\ln f$
CSFH Max. Likelihood (Optimized)	-2.78	-1518	51	50	-2.41
CSFH MCMC	$-2.81^{+0.05}_{-0.05}$	-1258^{+523}_{-669}	59^{+18}_{-12}	248^{+169}_{-171}	$-2.6^{+0.8}_{-0.7}$
SFH MCMC	···	-1087^{+561}_{-604}	73^{+22}_{-17}	242^{+168}_{-173}	···

2.5. *The MCMC solution*

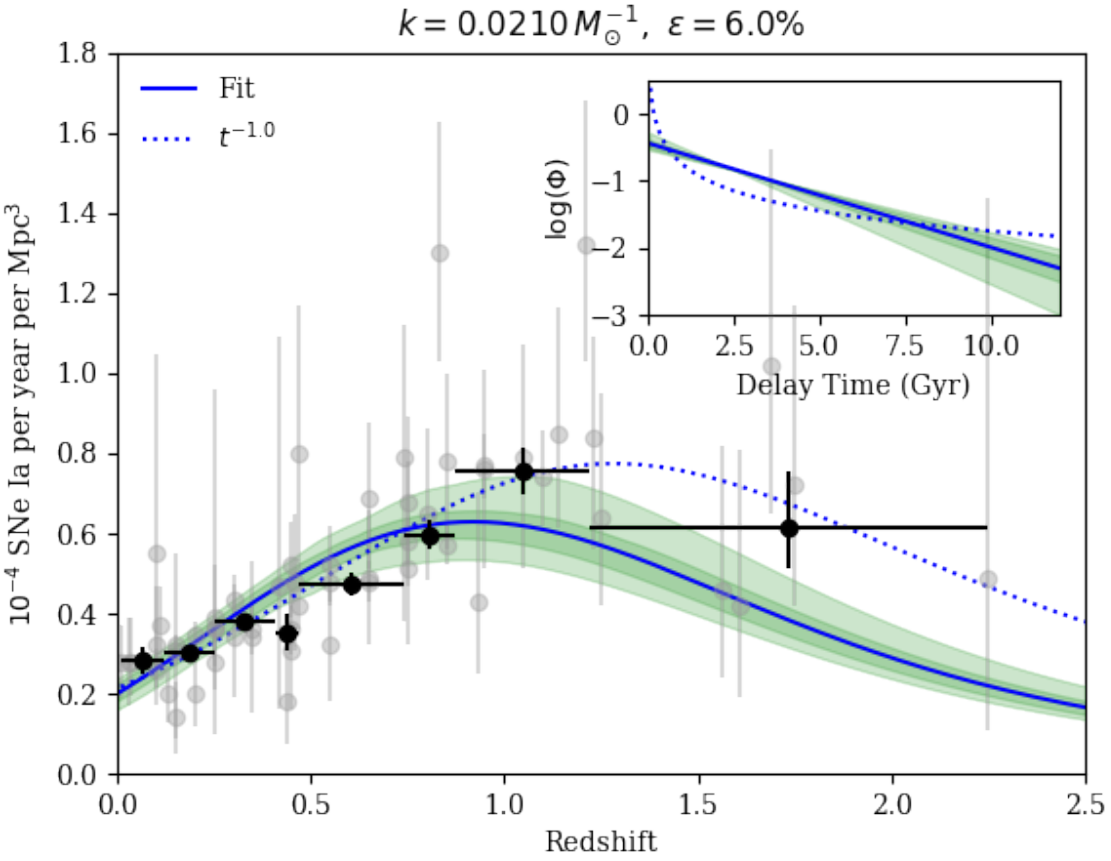

Figure 5. Similar to Figure 4, the $R_{\rm Ia}(z)$ result of from MCMC best-fit is shown (blue line), with the 68% and 95% confidence intevals, in dark and light green, respectively.

Exploring the parameter space in an MCMC allows both confirmation of the optimized solution and an exploration of the range of validity. We use the affine-invariant MCMC ensemble sampler from `emcee.py` (Foreman-Mackey et al. 2013) using the same likelihood function as shown in Equation 6, and set our uniform priors as described by the bounds, as shown in the previous section, with the exception of evaluating $\ln\varepsilon$ to allow MCMC step sizes of order unity, and using the prior $-10 < \ln\varepsilon < 0$. We then set 1,000 walkers to explore 10,000 steps, for a total of 10 million iterations, the first 100,000 of which we discard as 'burn-in'. The MCMC likelihood distributions are presented in the Appendix (Section A). The maximum-likelihood solution is shown in Figure 5 and tabulated in Table 4.

As these result show, there is a clear convergence in f, the factor by which reported statistical errors in rate measures are misestimated. Nearly all values are underestimated from as little as 4% to as much as 17%, with most only about $7-9$% underestimated. So, while there is a large dispersion in rate values, these values are reasonably consistent to within statistical errors, which are not grossly misestimated. The fraction ε is also very well constrained, and only 6.0 ± 0.3% of WD stars contribute as SN Ia progenitors.

However, the parameters which set the shape of the delay time distribution, ξ, ω, and α, appear very much less constrained by the MCMC. There is a clear maximum at $\omega \approx 60$ that is also highly degenerate with the value of ξ. And there does not appear to be any convergence or preference in the value of α. While it would appear there is no specific solution to the function, the resultant range in parameters indicate a family of solutions that are indeed related. Characterized by highly negative locations and broad widths, the only part of the distributions (in the 99% confidence interval) which lie in the positive time space are the exponential-like tails, as is shown in the inset of Figure 5.

3. DELAY TIME DISTRIBUTIONS FROM STAR FORMATION HISTORIES

Maoz et al. (2011) detailed a perscription for recovering delay-time distributions from an analysis of star-formation histories of the individual galaxies, both those which host supernova and those that do not, in the duration of a continuous survey. This is an evaluation of the maximum likelihood delay time distribution following the same approach, but performed on the GOODS/CANDELS SN hosts and other field galaxies. For this analysis we use star formation histories derived using the Bayesian modeling approach of Pacifici et al. (2012). In summary, the galaxy physical properties are retrieved from a combined analysis of stellar and nebular emission utilizing an extensive library of star formation and chemical enrichment histories. These libraries build a large repository of rest-frame galaxy spectral energy distributions, which are then used to determine likelihood distributions of physical parameters from a Bayesian analysis of observed spectral energy distributions. This is method has been applied to the HST/WFC3-F160W-selected CANDELS catalogs for the GOODS-South (Guo et al. 2013), and the GOODS-North (Barro et al., in preparation), into SFH catalogs (see Pacifici et al. 2016). We adopt only the median derived SFH of each galaxy for simplicity in this analysis.

For a given galaxy, the rate history of SNe Ia per year (r_i) would be:

$$r_i(t) = h^2\, k\, \varepsilon \int_0^t \Psi_i(t')\, \Phi(t - t')\, dt', \tag{8}$$

where Ψ_i is the star formation history of the galaxy (mapped in look-forward time), and Φ is the global delay time distribution model, also in look-forward time. The product of the rate at the observed epoch (r_i) and the observed control time ($t'_{c,i}$) for the galaxy– which contains all the information on the temporal sampling and depth of the survey– give the expected number of observed SN Ia events (m_i) over the duration of the survey by

$$m_i = r_i\, t'_{c,i}. \tag{9}$$

The probability distribution of those observed events is likely Poisson, where the likelihood of catching n_i SNe Ia from a galaxy when m_i are expected is

$$P(n_i|m_i) = \frac{m_i^{n_i} e^{-m_i}}{n_i!}. \tag{10}$$

The product of probabilities for all galaxies in the survey would then serve as the likelihood of a given rate model, tuned by the chosen delay-time distribution model. The log-likelihood, which is convenient for MCMCs, is then expressed by:

$$L = \prod_i^N P(n_i|M_i) \Rightarrow \ln L = -\sum^N m_i + \sum^N \ln\left(\frac{m_i^{n_i}}{n_i!}\right) \tag{11}$$

in which the last term is zero for the galaxies which did not host SNe Ia during the survey.

Using the control times derived for each survey field using the methods described in Strolger et al. (2015), Figure 6 shows examples "SN Ia rate history" one would derive from Equation 8 using the best-fit model from the MCMC on CSFHs, done in the previous section. The figure shows star-formation histories for two SN Ia host galaxies, for SN 2002hp and SN 2003dy, respectively (see Strolger et al. 2004, for further details on these events). Both galaxies are at $z \approx 1.3$, and in the GOODS-South and GOODS-North fields, respectively. The host of SN 2002hp is a fast-forming/slow-quenching passive galaxy that underwent a very large burst of star formation just a few Gyr ago, that when convolved with the applied delay time distribution results in a relatively large expected rate of 0.93 SNe Ia per millennium at the observed epoch. Conversely, the host of SN 2003dy is actively star forming at the observed epoch, albeit at a more modest rate, and has been active over the last few Gyr. The result is a SN Ia rate about three times larger, 2.94 per millennium, at the observed epoch. Nearly all non-hosts have predicted SN Ia rates at their respective observed epochs several orders of magnitude smaller than these two example hosts with this assumed $\Phi(t)$.

The SFH catalog contains 70,375 galaxies in the GOODS-North and South fields, selected with $H > 26$ mag (AB). There are 34 events classified as SNe Ia in the GOODS-South field, and 39 in the North field (Strolger et al. 2004; Dahlen et al. 2008; Rodney et al. 2014), all but 6 of which were matched to host galaxies in the SFH catalog. Two of these hosts were rejected as their events spectroscopic redshifts were very inconsistent with the SFH catalog redshifts, and the other 4 were simply not matched to galaxies in the SFH catalog, as they were either too faint or too near the field edge to be listed in the composite photometry catalogs. Cumulative distribution functions for the total masses and star formation rates (in the observed epoch) of the SN Ia hosts relative to the population of catalog galaxies are shown in Figure 7. Two-sided KS tests on the CDFs by mass and star formation rates do not reject the null hypothesis

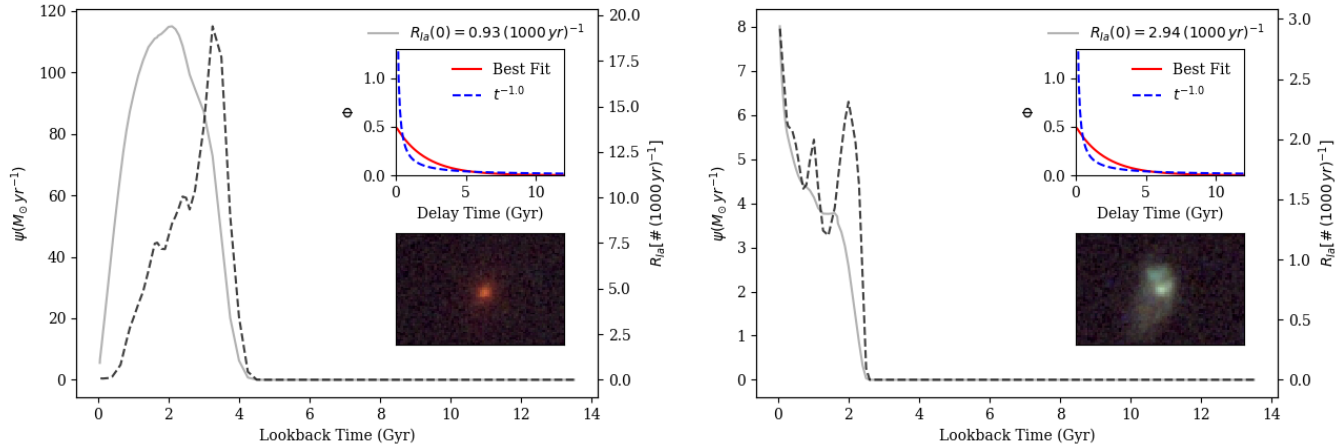

Figure 6. Example star formation histories (dashed-line and left ordinate), and the resultant SN Ia rate histories (dotted-line and right ordinate) for two SN Ia host galaxies in our sample, SNe 2002hp (left) and 2003dy (right), in the GOODS-South and GOODS-North fields, respectively. Insets show the delay time distribution applied (upper right, in red) compared to t^{-1} (blue dashed), and a three-color HST ACS/WFC image (lower right) of the SN host galaxy.

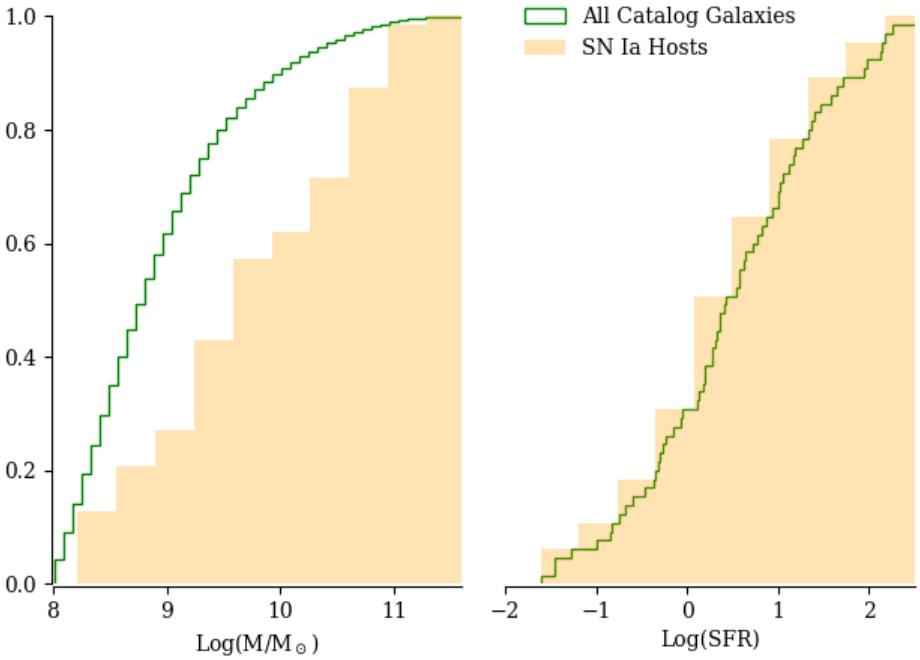

Figure 7. CDFs for the total masses (left) and star formation rates (SFR; right) for the 66 SN Ia hosts (yellow), compared to the 70,375 catalog galaxies (green). KS tests on each suggest the population of SN Ia hosts are statistically consistent (to the $> 95\%$ and $> 99\%$ level, respectively) with the rest of the catalog.

to $> 95\%$ and $> 99\%$, respectively, implying the population of SN Ia hosts are statistically consistent with the rest of the catalog.

The model parameters, ξ, ω, and α are then explorable via `emcee.py`. We keep the same uniform priors as bounds, as described in Sections 2.4 and 2.5. We fix the fraction $\varepsilon = 0.06$ for convenience, and set 100 walkers exploring 500 steps on these parameters, the first 50 of which are discarded as burn-in. The maximum likelihood results for the

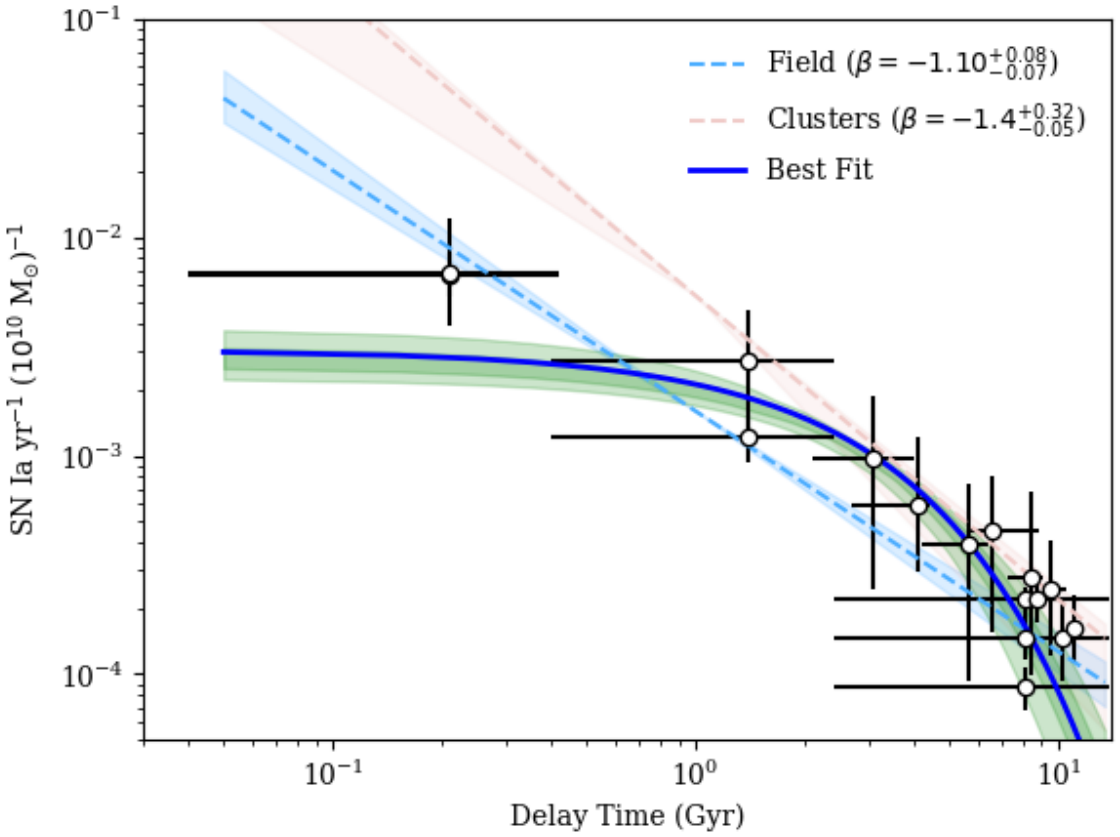

Figure 8.

45,000 iterations on SFHs are identical to the results for the CSFH assessment presented in Section 2.2, as is shown and Table 4. The MCMC likelihood distributions are presented in the Appendix (Section A).

4. DISCUSSION

All three methods point to a family of delay-time distribution models that are somewhat similar to power-law models, but are more exponential, having much fewer prompt events in the 40 Myr to 1 Gyr range. The model also helps to clarify a discussion of 'prompt' vs 'delayed' progenitor mechanism.

It is useful to evaluate the SN Ia rate that would result from the average galaxy (approx. 10^{10} M$_\odot$), undergoing a single, 1 M$_\odot$ yr^{-1} burst of star formation, and the number of SNe Ia per year that would result over time. Figure 8 shows the DTDs recovered in various time bins from Sloan galaxy data Maoz et al. (2010, 2011, 2012); Graur & Maoz (2013) along with the derived power-law DTD models for field and galaxy cluster hosts. Rather than suggesting different power-law slopes, our best-fit DTD connects the data in clustered and field environments.

The Hubble-time integrated SN Ia production efficiency, combining the k and ε terms, yields $N/M_\star = 1.26$ events per 1000 M$_\odot$ formed.

APPENDIX

A. RATES FROM

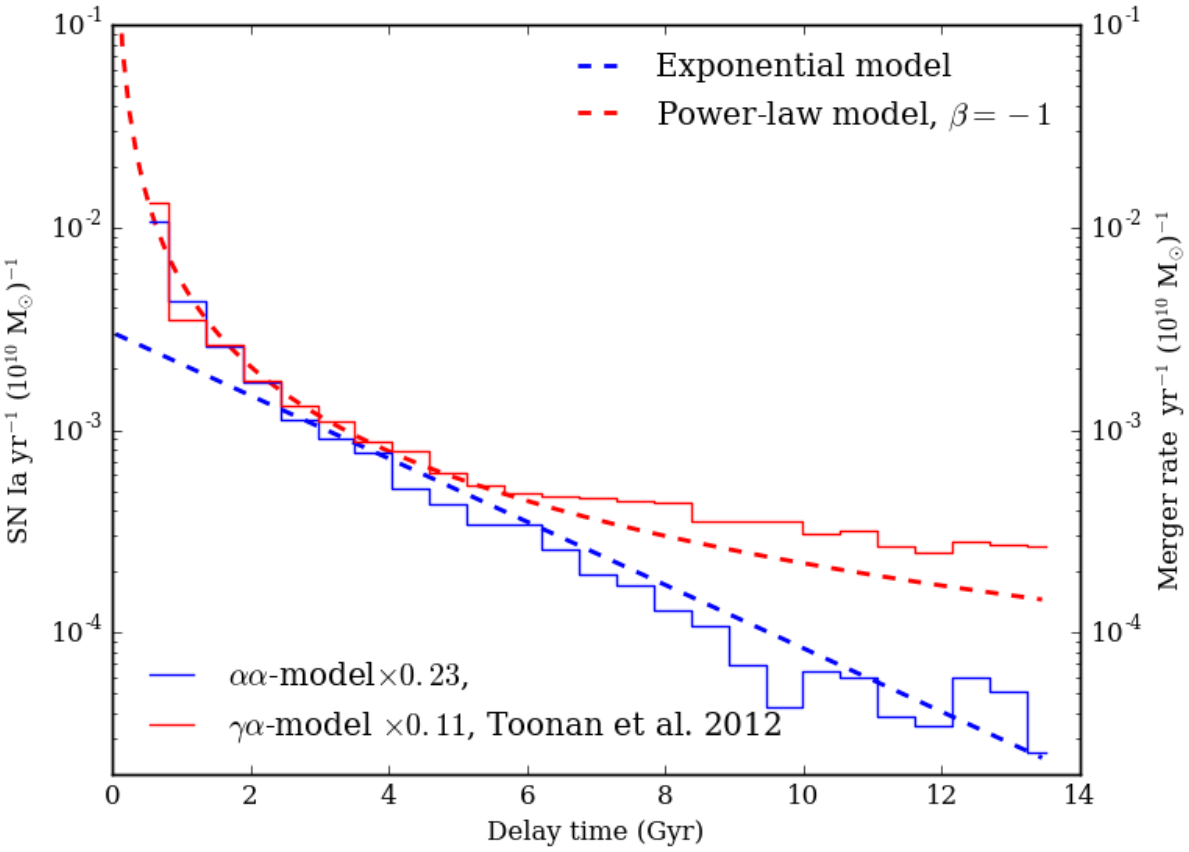
Exponential model
Power-law model, $\beta = -1$
$\alpha\alpha$-model $\times 0.23$,
$\gamma\alpha$-model $\times 0.11$, Toonan et al. 2012
SN Ia yr^{-1} (10^{10} M$_\odot$)$^{-1}$
Merger rate yr^{-1} (10^{10} M$_\odot$)$^{-1}$
Delay time (Gyr)
10^{-1}
10^{-2}
10^{-3}
10^{-4}
0
2
4
6
8
10
12
14

Figure 9.

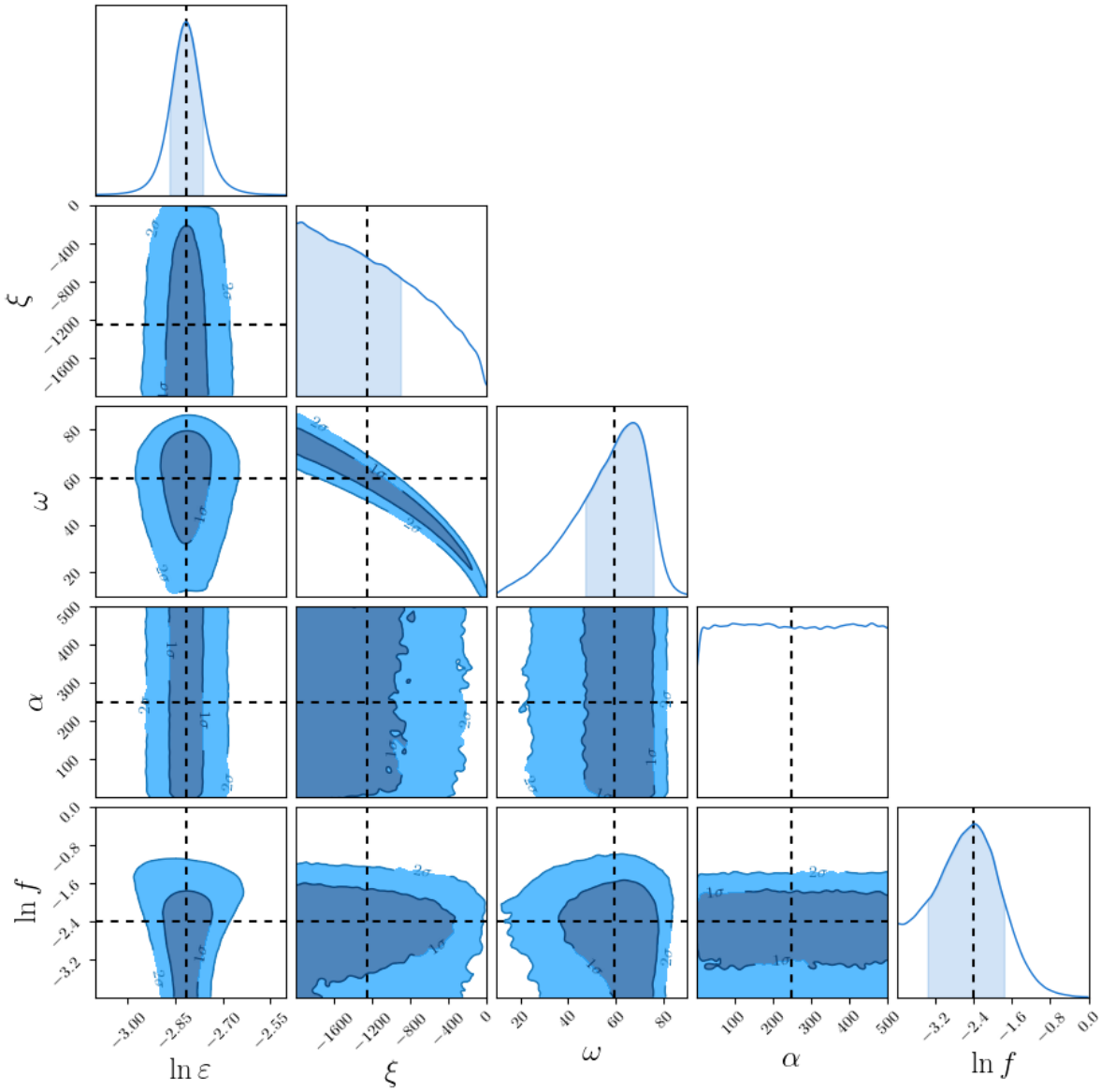

Figure 10. MCMC results on the parameters of a unimodal delay-time distribution model, fit to volumetric rate data and CSFH. Dashed lines indicate the maximum likelihood values. The $1-\sigma$ and $2-\sigma$ regions about those best fits are shown in dark and light blue, respectively. The plot generated using `ChainConsumer.py` (Hinton 2016).

Table 5. Parameter Covariance MCMC SFD

	f	ξ	ω	α	$\log\phi$
f	0.41	-125.69	6.61	33.98	-0.41
ξ	-125.69	412816.10	-14898.10	-52398.20	518.74
ω	6.61	-14898.10	660.60	2209.32	-22.89
α	33.98	-52398.20	2209.32	27290.24	-131.67
$\log\phi$	-0.41	518.74	-22.89	-131.67	2.35

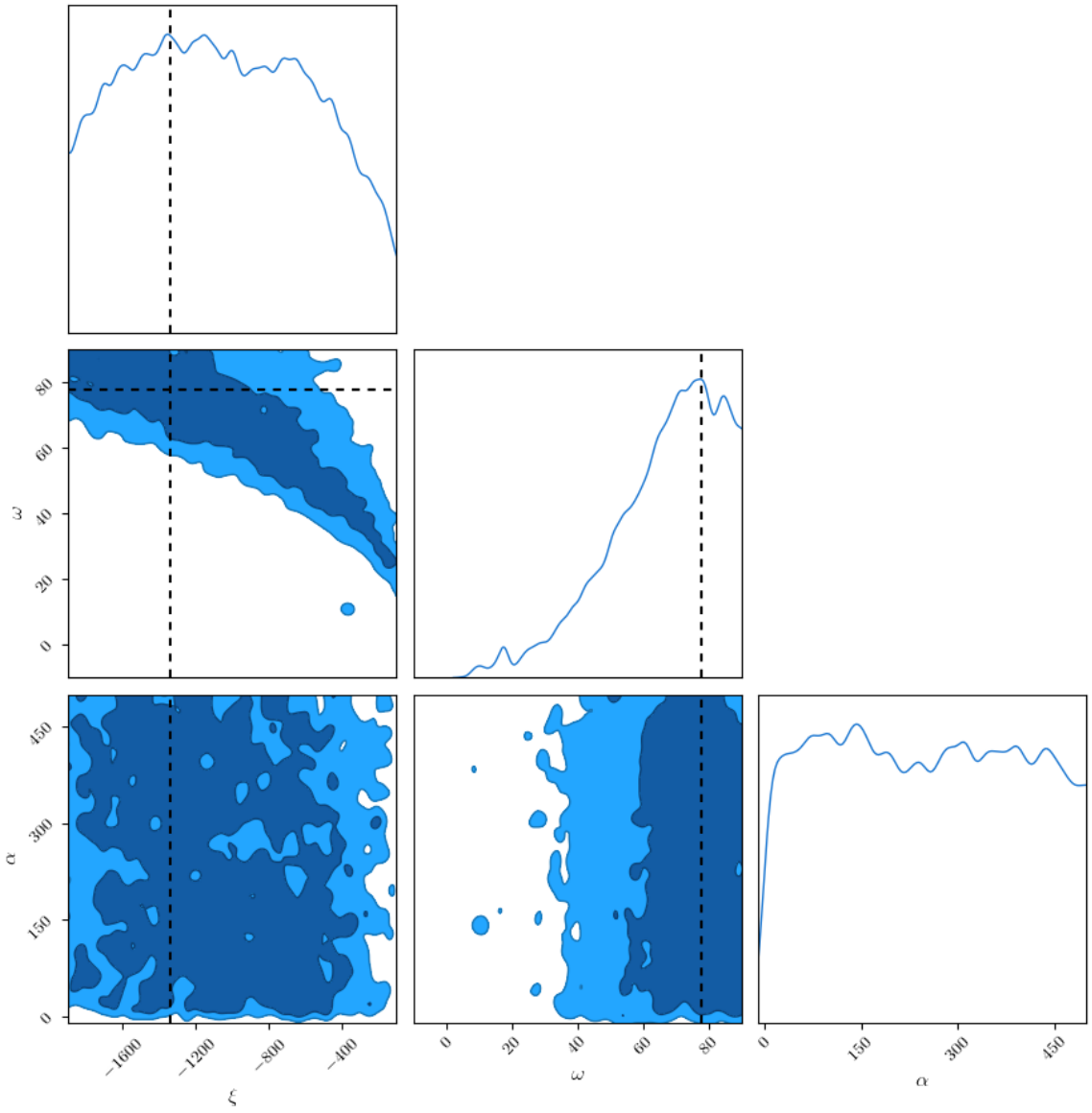

Figure 11. MCMC results on unimodal delay-time distribution model, fit to SFHs for 33,678 galaxies in the GOODS fields, 67 of which are SN Ia hosts.

REFERENCES

Arnett, W. D. 1969, Ap&SS, 5, 180, doi: 10.1007/BF00650291

Blanc, G., Afonso, C., Alard, C., et al. 2004, A&A, 423, 881, doi: 10.1051/0004-6361:20035948

Table 6. Parameter Covariance MCMC SFD

	f	ξ	ω	α	$\log\phi$
f	0.41	-125.69	6.61	33.98	-0.41
ξ	-125.69	412816.10	-14898.10	-52398.20	518.74
ω	6.61	-14898.10	660.60	2209.32	-22.89
α	33.98	-52398.20	2209.32	27290.24	-131.67
$\log\phi$	-0.41	518.74	-22.89	-131.67	2.35

Botticella, M. T., Riello, M., Cappellaro, E., et al. 2008, A&A, 479, 49

Bouwens, R. J., Illingworth, G. D., Oesch, P. A., et al. 2015, ApJ, 803, 34, doi: 10.1088/0004-637X/803/1/34

Brandt, T. D., Tojeiro, R., Aubourg, É., et al. 2010, AJ, 140, 804, doi: 10.1088/0004-6256/140/3/804

Breedt, E., Steeghs, D., Marsh, T. R., et al. 2017, MNRAS, 468, 2910, doi: 10.1093/mnras/stx430

Cappellaro, E., Evans, R., & Turatto, M. 1999, A&A, 351, 459

Cappellaro, E., Turatto, M., Benetti, S., et al. 1993, A&A, 273, 383+

Cappellaro, E., Botticella, M. T., Pignata, G., et al. 2015, A&A, 584, A62, doi: 10.1051/0004-6361/201526712

Catalán, S., Isern, J., García-Berro, E., & Ribas, I. 2008, MNRAS, 387, 1693, doi: 10.1111/j.1365-2966.2008.13356.x

Chen, M. C., Herwig, F., Denissenkov, P. A., & Paxton, B. 2014, Monthly Notices of the Royal Astronomical Society, 440, 1274, doi: 10.1093/mnras/stu108

Croton, D. J. 2013, Publications of the Astronomical Society of Australia, 30, e052, doi: 10.1017/pasa.2013.31

Cummings, J. D., Kalirai, J. S., Tremblay, P.-E., Ramirez-Ruiz, E., & Choi, J. 2018, ArXiv e-prints. https://arxiv.org/abs/1809.01673

Dahlen, T., Strolger, L.-G., & Riess, A. G. 2008, ApJ, 681, 462, doi: 10.1086/587978

Denissenkov, P. A., Truran, J. W., Herwig, F., et al. 2015, Monthly Notices of the Royal Astronomical Society, 447, 2696, doi: 10.1093/mnras/stu2589

Dilday, B., Smith, M., Bassett, B., et al. 2010, ApJ, 713, 1026, doi: 10.1088/0004-637X/713/2/1026

Driver, S. P., Andrews, S. K., da Cunha, E., et al. 2018, MNRAS, 475, 2891, doi: 10.1093/mnras/stx2728

Finkelstein, S. L., Ryan, Jr., R. E., Papovich, C., et al. 2014, ArXiv e-prints. https://arxiv.org/abs/1410.5439

Foreman-Mackey, D., Hogg, D. W., Lang, D., & Goodman, J. 2013, PASP, 125, 306, doi: 10.1086/670067

Graur, O., & Maoz, D. 2013, MNRAS, 689, doi: 10.1093/mnras/sts718

Graur, O., Poznanski, D., Maoz, D., et al. 2011, MNRAS, 417, 916, doi: 10.1111/j.1365-2966.2011.19287.x

Graur, O., Rodney, S. A., Maoz, D., et al. 2014, ApJ, 783, 28, doi: 10.1088/0004-637X/783/1/28

Guo, Y., Ferguson, H. C., Giavalisco, M., et al. 2013, The Astrophysical Journal Supplement Series, 207, 24, doi: 10.1088/0067-0049/207/2/24

Hinton, S. R. 2016, The Journal of Open Source Software, 1, 00045, doi: 10.21105/joss.00045

Hogg, D. W., Bovy, J., & Lang, D. 2010, ArXiv e-prints. https://arxiv.org/abs/1008.4686

Horesh, A., Poznanski, D., Ofek, E. O., & Maoz, D. 2008, MNRAS, 389, 1871, doi: 10.1111/j.1365-2966.2008.13697.x

Hounsell, R., Scolnic, D., Foley, R. J., et al. 2018, ApJ, 867, 23, doi: 10.3847/1538-4357/aac08b

Iben, Jr., I., & Tutukov, A. V. 1984, ApJS, 54, 335, doi: 10.1086/190932

Khusanova, Y., Fèvre, O. L., Cassata, P., et al. 2019, arXiv e-prints, arXiv:1903.01884. https://arxiv.org/abs/1903.01884

Kroupa, P. 2001, MNRAS, 322, 231, doi: 10.1046/j.1365-8711.2001.04022.x

Li, W., Chornock, R., Leaman, J., et al. 2011, MNRAS, 412, 1473, doi: 10.1111/j.1365-2966.2011.18162.x

Madau, P., & Dickinson, M. 2014, ARA&A, 52, 415, doi: 10.1146/annurev-astro-081811-125615

Madgwick, D. S., Hewett, P. C., Mortlock, D. J., & Wang, L. 2003, ApJL, 599, L33, doi: 10.1086/381081

Mannucci, F., Della Valle, M., Panagia, N., et al. 2005, A&A, 433, 807, doi: 10.1051/0004-6361:20041411

Maoz, D., & Graur, O. 2017, ApJ, 848, 25, doi: 10.3847/1538-4357/aa8b6e

Maoz, D., & Hallakoun, N. 2017, MNRAS, 467, 1414, doi: 10.1093/mnras/stx102

Maoz, D., & Mannucci, F. 2012, PASA, 29, 447, doi: 10.1071/AS11052

Maoz, D., Mannucci, F., & Brandt, T. D. 2012, MNRAS, 426, 3282, doi: 10.1111/j.1365-2966.2012.21871.x

Maoz, D., Mannucci, F., Li, W., et al. 2011, MNRAS, 412, 1508, doi: 10.1111/j.1365-2966.2010.16808.x

Maoz, D., Mannucci, F., & Nelemans, G. 2013, ArXiv e-prints. https://arxiv.org/abs/1312.0628

Maoz, D., Sharon, K., & Gal-Yam, A. 2010, ApJ, 722, 1879, doi: 10.1088/0004-637X/722/2/1879

Napiwotzki, R., Karl, C. A., Nelemans, G., et al. 2007, in Astronomical Society of the Pacific Conference Series, Vol. 372, 15th European Workshop on White Dwarfs, ed. R. Napiwotzki & M. R. Burleigh, 387. http://adsabs.harvard.edu/abs/2007ASPC..372..387N

Neill, J. D., Sullivan, M., Balam, D., et al. 2006, AJ, 132, 1126, doi: 10.1086/505532

Nelemans, G., Portegies Zwart, S. F., Verbunt, F., & Yungelson, L. R. 2001a, A&A, 368, 939, doi: 10.1051/0004-6361:20010049

Nelemans, G., Toonen, S., & Bours, M. 2013, in IAU Symposium, Vol. 281, IAU Symposium, 225–231

Nelemans, G., Yungelson, L. R., Portegies Zwart, S. F., & Verbunt, F. 2001b, A&A, 365, 491, doi: 10.1051/0004-6361:20000147

Nomoto, K. 1982, ApJ, 253, 798, doi: 10.1086/159682

Okumura, J. E., Ihara, Y., Doi, M., et al. 2014, ArXiv e-prints. https://arxiv.org/abs/1401.7701

Öpik, E. 1924, Publications of the Tartu Astrofizica Observatory, 25, 1

Pacifici, C., Charlot, S., Blaizot, J., & Brinchmann, J. 2012, MNRAS, 421, 2002, doi: 10.1111/j.1365-2966.2012.20431.x

Pacifici, C., Kassin, S. A., Weiner, B. J., et al. 2016, ApJ, 832, 79, doi: 10.3847/0004-637X/832/1/79

Pain, R., Fabbro, S., Sullivan, M., et al. 2002, ApJ, 577, 120

Perlmutter, S., Aldering, G., Goldhaber, G., et al. 1999, ApJ, 517, 565, doi: http://dx.doi.org/10.1086/307221

Perrett, K., Sullivan, M., Conley, A., et al. 2012, AJ, 144, 59, doi: 10.1088/0004-6256/144/2/59

Riess, A. G., Filippenko, A. V., Challis, P., et al. 1998, AJ, 116, 1009, doi: 10.1086/300499

Rodney, S. A., & Tonry, J. L. 2010, ApJ, 723, 47, doi: 10.1088/0004-637X/723/1/47

Rodney, S. A., Riess, A. G., Strolger, L.-G., et al. 2014, AJ, 148, 13, doi: 10.1088/0004-6256/148/1/13

Salpeter, E. E. 1955, ApJ, 121, 161, doi: 10.1086/145971

Strolger, L., Dahlen, T., & Riess, A. G. 2010, ApJ, 713, 32, doi: 10.1088/0004-637X/713/1/32

Strolger, L. G. 2003, PhD thesis, University of Michigan

Strolger, L.-G., Riess, A. G., Dahlen, T., et al. 2004, ApJ, 613, 200

Strolger, L.-G., Dahlen, T., Rodney, S. A., et al. 2015, ApJ, 813, 93, doi: 10.1088/0004-637X/813/2/93

Takahashi, K., Yoshida, T., & Umeda, H. 2013, ApJ, 771, 28, doi: 10.1088/0004-637X/771/1/28

Tonry, J. L., Schmidt, B. P., Barris, B., et al. 2003, ApJ, 594, 1, doi: 10.1086/376865

Wang, B., & Han, Z. 2012, NewAR, 56, 122, doi: 10.1016/j.newar.2012.04.001

Webbink, R. F. 1984, ApJ, 277, 355, doi: 10.1086/161701

Whelan, J., & Iben, I. J. 1973, ApJ, 186, 1007, doi: 10.1086/152565